EUROPHYSICS LETTERS ? ? 1999

Europhys. Lett., **?** (?), pp. 1-∞ (1999)

arXiv:cond-mat/9907224v1 15 Jul 1999

Vortex structures in dilute quantum fluids

T. WINIECKI[1], J. F. MCCANN[2], and , C. S. ADAMS[1]

[1] *Dept. of Physics, University of Durham, Rochester Building, South Road, Durham, DH1 3LE, England. UK.*

[2] *Dept. of Applied Mathematics and Theoretical Physics, Queen's University, Belfast, BT7 1NN, Northern Ireland. UK.*

(received ; accepted)

PACS. 02.30 – Nonlinear differential equations.
PACS. 03.75.F – Bose-Einstein condensation.
PACS. 47.37.+q– Superfluid hydrodynamics.
PACS. 67.40.Vs – Vorticity in ^{4}He.

Abstract. – Vortex structures in dilute quantum fluids are studied using the Gross-Pitaevskii equation. The velocity and momentum of multiply quantized vortex rings are determined and their core structures analysed. For flow past a spherical object, we study the encircling and pinned ring solutions, and determine their excitation energies as a function of the flow velocity for both penetrable and impenetrable objects. The ring and laminar flow solutions converge at a critical velocity, which decreases with increasing object size. We also study the vortex solutions associated with flow past a surface bump which indicate that surface roughness also reduces the critical velocity. This effect may have important implications for the threshold of dissipation in superfluids and superconductors.

Introduction. – The breakdown of superfluidity in liquid helium (HeII) [1, 2], dissipation in superconductors [2], and topological defects in cosmology [3] all involve vortices. Given their prevalence, it is perhaps surprising how little is known about their structure and the exact mechanism of their formation. For example, in HeII vortex rings can be produced experimentally by injecting ions into the fluid [1, 2]. However, it is not known whether the rings emerge via *quantum transition*, where the ion creates an encircling ring and subsequently attaches itself to the vortex core; or *peeling*, where the ion creates a vortex loop which grows to form a pinned ring [1, 2]. In principle, this question could be addressed by simulation, except that a complete hydrodynamical model of HeII has yet to be established. One can formulate a simple model of a dilute Bose fluid based on the Gross-Pitaevskii or non-linear Schrödinger equation (NLSE) [4]. This approach can be expected to provide an accurate quantitative description in the case of dilute Bose-Einstein condensates [5], and offer considerable insight into the physics of HeII. Vortex solutions of the NLSE equation have been studied for a number of simple geometries: Flow past an object has been studied in one [6] and two dimensions [7], and it is found that stationary vortex solutions exist only for motion slower a critical velocity. Above this velocity, one observes the periodic emission of vortices leading to a pressure imbalance which produces drag on the object [8]. Consequently, the critical velocity also determines the transition between superfluid and normal flow.

In this paper, we investigate stationary vortex solutions near an object in three dimensions. For a spherical object, there are two solutions: the *encircling ring*, where the object is positioned at the centre of the ring; and the *pinned ring*, where the object centre lies within the core of the vortex line. For all object potentials laminar flow evolves smoothly into the encircling ring solution suggesting that the quantum transition model of ring nucleation is favoured. Finally, we study flows parallel to a plane and illustrate the effect of surface roughness on the critical velocity.

Numerical method. – Consider an object described by a potential $V(\boldsymbol{r})$ moving with velocity $\boldsymbol{v}$ through a fluid of interacting bosons with mass m and uniform asymptotic number density n_0. In the fluid rest frame, $\boldsymbol{r}' = \boldsymbol{r} + \boldsymbol{v}t$, the dynamics can be described in terms of the order parameter, $\psi(\boldsymbol{r}', t)$, which is a solution of the NLSE,

$$i\hbar \frac{\partial}{\partial t}\psi(\boldsymbol{r}', t) = -\frac{\hbar^2}{2m}\nabla'^2\psi(\boldsymbol{r}', t) + V(\boldsymbol{r}' - \boldsymbol{v}t)\psi(\boldsymbol{r}', t) + C|\psi(\boldsymbol{r}', t)|^2\psi(\boldsymbol{r}', t) \ , \tag{1}$$

where the nonlinear coefficient, $C = 4\pi\hbar^2 a/m$, and a is the s-wave scattering length. If distance and velocity are measured in terms of the healing length, $\xi = \hbar/\sqrt{mn_0C}$, and the speed of sound, $c = \sqrt{n_0C/m}$, respectively, and the asymptotic number density is rescaled to unity, then Eq. (1) in the frame of the object becomes

$$i\partial_t\psi = -\tfrac{1}{2}\nabla^2\psi + V\psi + |\psi|^2\psi + i\boldsymbol{v}\cdot\nabla\psi \ . \tag{2}$$

Stationary states, $\psi(\boldsymbol{r}, t) = \mathrm{e}^{-i\mu t}\phi(\boldsymbol{r})$, corresponding to a chemical potential, $\mu = 1$, are found by numerical solution of the discretized system of equations. In the special case of rotational symmetry about the axis of flow, the problem can be solved using 2D cylindrical polar coordinates (ρ, z). In the general case, we use a cartesian 3D grid $\phi(\boldsymbol{r}) = \phi(x, y, z)$. Defining $\phi_{ijk0} = \Re(\phi(x_i, y_j, z_k))$ and $\phi_{ijk1} = \Im(\phi(x_i, y_j, z_k))$, and taking the flow direction to define the z-axis, Eq. (2) becomes

$$\begin{aligned} f_{ijkr} \equiv & -\left(\phi_{i+1jkr} + \phi_{i-1jkr} + \phi_{ij+1kr} + \phi_{ij-1kr} + \phi_{ijk+1r} + \phi_{ijk-1r} - 6\phi_{ijkr}\right)/2\Delta^2 \\ & + V_{ijk}\phi_{ijkr} + \left(\phi_{ijk0}^2 + \phi_{ijk1}^2\right)\phi_{ijkr} - \phi_{ijkr} + (2r-1)v(\phi_{ijk+1,1-r} - \phi_{ijk-1,1-r})/2\Delta = 0 \end{aligned} \tag{3}$$

where Δ is the grid spacing (values of Δ between 0.125 and 0.4 were used). The solution of these equations is found using the linearization

$$f_{ijkr}(\phi_{lmns}^{(p)}) + \sum_{lmns}\left(\phi_{lmns}^{(p+1)} - \phi_{lmns}^{(p)}\right)\left[\frac{\partial f_{ijkr}}{\partial \phi_{lmns}}\right]^{(p)} \approx 0 \ , \tag{4}$$

where $\phi^{(p+1)}$ is determined from the approximation $\phi^{(p)}$ by solving Eq. (4) using the biconjugate gradient method [9]. Large box sizes $(0 \le x \le \infty)$ are simulated by employing the nonlinear transformation $\hat{x} = x/(x + D)$, where D is chosen to give sufficient point coverage within the healing length. The iterative solution depends on the initial guess $\phi^{(0)}$; for example, laminar flows are found by choosing $\phi^{(0)} = \mu = 1$, whereas vortex solutions are found by imposing the vortex phase pattern on $\phi^{(0)}$, and then relaxing the imposed phase after a few iterations.

Free vortex rings. – For an unbounded flow $(V = 0)$ one finds free vortex rings. Fig. 1 shows a surface plot of ring solutions with circulation, $\kappa = 2\pi$, 4π, and 6π. The double $(\kappa = 4\pi)$

and triple ($\kappa = 6\pi$) rings only exist for $v > 0.56$ and $v > 0.67$, and their cores consists of 2 and 3 lines of zero density, respectively. The separation of the density minima depends on the radius, increasing up to about two healing lengths for $R = 5$. For $\kappa = 6\pi$, the central minima has a larger radius. Similar core structures are also found in the corresponding 2D solutions. Although vortex rings with multiple circulation have higher energy ($E \propto \kappa^2$) than the corresponding number of single rings ($E \propto \kappa$), we find that they are stable when subject to a perturbation in a time-dependent simulation (similar robustness has also been found for vortex lines with multiple circulation [10]). Fig. 2 shows a plot of the velocity (equivalent to the ring propagation velocity in a stationary fluid) and momentum as a function of ring radius, R. For $R > 5$, the velocity can predicted accurately by $v = \kappa\left[\ln(8R/a) - b\right]/4\pi R$, where a is

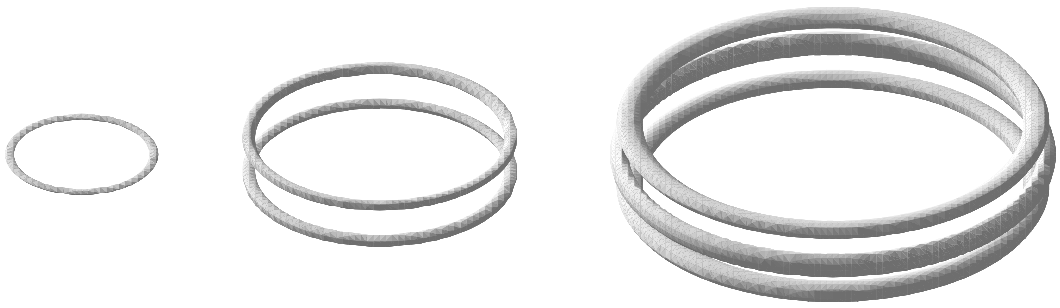

Fig. 1. – Surface density ($|\phi|^2 = 0.02$) of vortex rings with $\kappa = 2\pi$, 4π, and 6π for $v = 0.5$. The flow direction is parallel to the axis of the rings. The core structure is only visible at very low density: the surface density plot for $|\phi|^2 = 0.08$ appears as a single ring in each case.

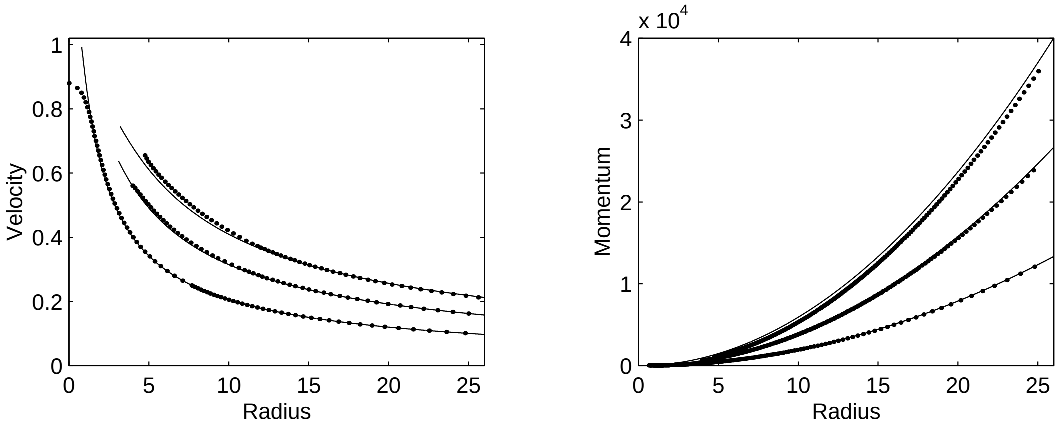

Fig. 2. – Vortex ring velocity (left) and momentum (right) for $\kappa = 2\pi$, 4π, and 6π: The numercial data ($\cdot$) are compared to $v = \kappa\left[\ln(8R/a) - b\right]/4\pi R$ ($a = 1/\sqrt{2}$, $b = 0.615$, 1.58, and 2.00), and $P = \pi\kappa R^2$, respectively.

the core radius ($a = 1/\sqrt{2}$ in our units) and b is a constant which depends on the structure of the core ($b = 0.25$ for a classical fluid, whereas $b = 0.615$ has been predicted for a dilute quantum fluid [11]). Numerical fits give $b = 0.615$ (as expected), 1.58, and 2.00 for $\kappa = 2\pi$, 4π and 6π, respectively. For $\kappa = 2\pi$ (single ring), the ring disappears (i.e. the on-axis density becomes zero) when $v = 0.88$, however, a solution other than laminar flow exists up to $v = 1.0$ (see below).

Flow past a sphere. – The free ring solutions discussed above are modified by the presence of an object or surface. In this section, we present results for a spherical object with radius R and potential height V, i.e., $V(r) = V$ $(r \leq R)$ and $V(r) = 0$ $(r > R)$. Fig. 3 shows surface density images of the three possible solutions: *laminar flow*; the *pinned ring* or *vortex loop*; and the *encircling ring* (the corresponding 2D solutions: laminar flow; a free and a bound vortex, and a vortex pair, were studied by Huepe and Brachet [7]). Fig. 4 shows a section of the velocity field pattern around the obstacle for each case. As the flow velocity increases, the vortices move closer to the object and eventually merge into the surface. Close to the critical velocity, the flow patterns converge (Fig. 4 lower).

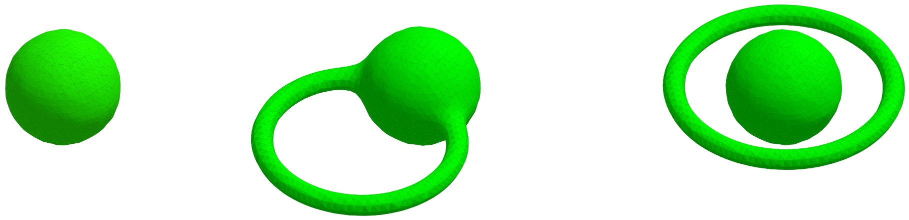

Fig. 3. – Surface density plots ($|\phi|^2 = 0.25$) showing the three steady-state solution associated with flow past a spherical object: from left to right, laminar flow; pinned ring; encircling ring.

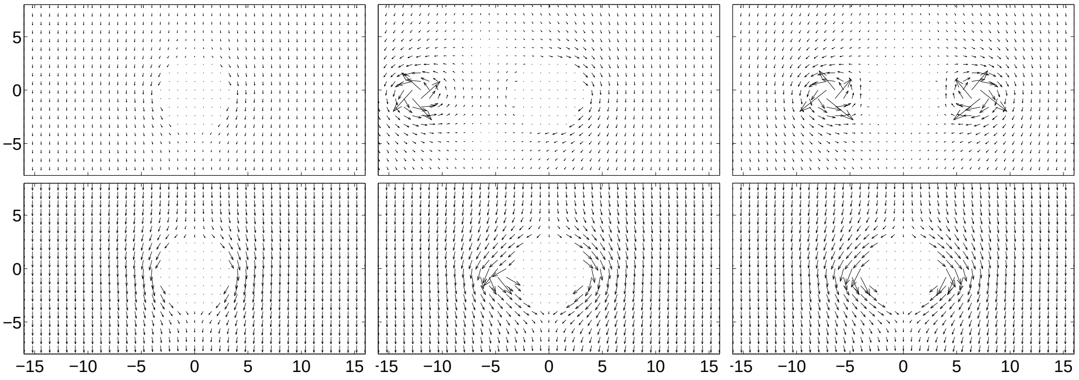

Fig. 4. – The velocity field pattern in the plane of a spherical object with radius $R = 3.3$ for $v = 0.3$ (above) and $v = 0.66$ (below) (the critical velocity, $v_c = 0.678$). The three columns correspond to laminar flow (left), the pinned ring (middle), and the encircling ring (right). Note the circulation around the object in the pinned ring solution. Only one quarter of actual grid points are shown.

Vortex energy. – The Lagrangian density of the NLSE (1) in scaled units, is given by

$$\mathcal{L}(\psi, \nabla\psi, \dot{\psi}) = i\psi^*\dot{\psi} - \frac{1}{2}\nabla\psi^*\nabla\psi - V\psi^*\psi - \frac{1}{2}\left(\psi^*\psi\right)^2 \ . \tag{5}$$

From the Hamiltonian, $H = \int \mathrm{d}\boldsymbol{r}[(\partial\mathcal{L}/\partial\dot{\psi})\dot{\psi} - \mathcal{L}]$, we define the energy relative to the ground state (i.e. laminar flow with $V = 0$ and having the same number of particles), as

$$E = \int \mathrm{d}\boldsymbol{r} \left\{ \frac{1}{2}\left|\nabla\phi\right|^2 + V\left|\phi\right|^2 + \frac{1}{2}\left(\left|\phi\right|^2 - 1\right)^2 \right\} \ . \tag{6}$$

Any deviation of the local particle density $\left|\phi\right|^2$ from 1 constitutes an excitation. Eq. (6) can be rewritten as

$$E = \int \mathrm{d}\boldsymbol{r} \left\{ \frac{1}{2}\left(1 - \left|\phi\right|^4\right) \right\} + \boldsymbol{v}\cdot\boldsymbol{P} \ , \tag{7}$$

where $\boldsymbol{P} = -i\int \mathrm{d}\boldsymbol{r}\,\{\phi^*\nabla\phi\}$ is ring momentum, and E and $\boldsymbol{P}$ are measured in units of $\hbar n_0 c\xi^2$ and $\hbar n_0\xi^2$, respectively. The energy as a function of flow velocity for different obstacle heights is shown in Fig. 5. With no object ($V = 0$), Fig. 5(upper left), the energy of the ring decreases

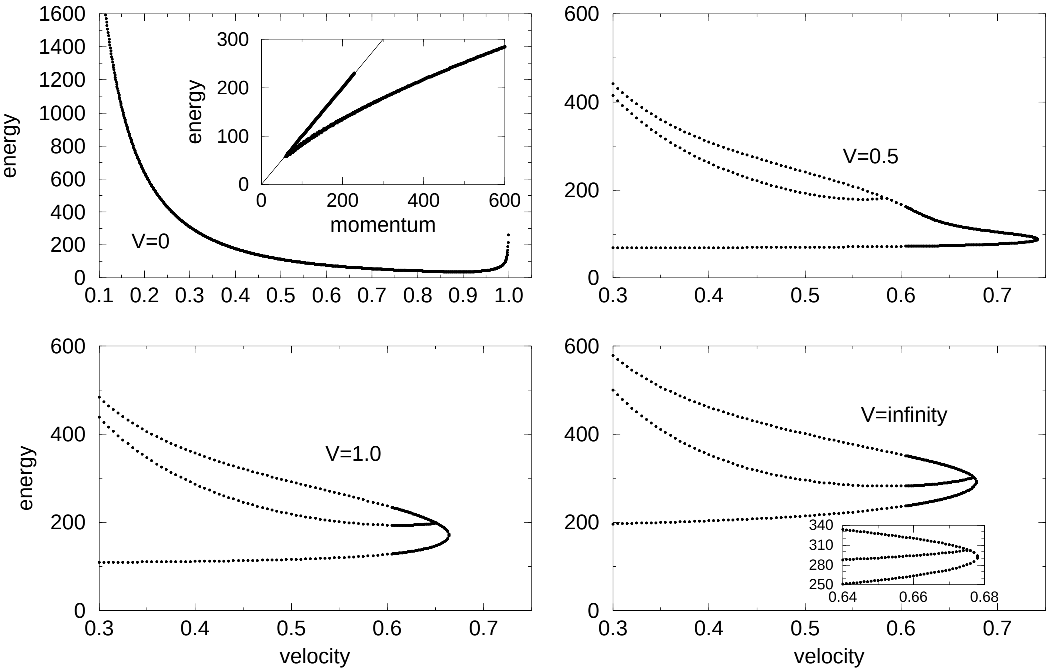

Fig. 5. – The energy of the stationary solutions of the NLSE as a function of the flow velocity. With no obtacle (upper left) 'ring' solutions are found up to the speed of sound $v = 1.0$. The ring collapses at $v = 0.88$ leaving a localised solitary wave with energy, $E \sim cP$ (see inset). If a sphere ($R = 3.3$) is inserted in the flow, the ring solution splits into a pinned and an encircling ring (higher energy). Even for $V = \infty$, the encircling and pinned solutions merge below the critical velocity (inset, lower right).

with increasing velocity reaching a minimum at $v = 0.93$, which coressponds to the cusp in the dispersion curve (see inset). For $v > 0.93$, the collapsed ring leaves a lower density, higher velocity region with energy $E \sim cP$, christened a rarefraction pulse by Jones and Roberts [12]. Inserting $E = cP$ in Eq. (7), one finds that as v decreases, $|\phi|^2$ must also decrease, but this becomes impossible when $|\phi|^2 = 0$, so the rarefraction pulse is replaced by a vortex ring. The process of supersonic flow creating a localised sound wave which evolves into a vortex ring (or pair in 2D) appears to be central to the mechanism of vortex nucleation in dilute quantum fluids (see e.g. Fig. 4 in Ref. [13]). For $V > 0$, the energy of the laminar flow solution is no longer zero, and the ring solution splits into two branches corresponding to the pinned ring and the encircling ring (Fig. 5 upper right). For low velocities (large radii), the energy of the encircling ring is higher than the pinned ring by an amount corresponding to the energy of the ring segment inside the object. Note that the pinned and encircling ring solutions always merges below the critical velocity, Fig. 5 lower right (inset). In a time-dependent simulation we observe a smooth transition (with no energy barrier) between laminar flow and the encircling ring supporting the quantum transition model of ring formation [1, 2].

Flow adjacent to a plane boundary. – For flow adjacent to a plane boundary, three classes of solution may be distinguished: laminar flow; vortex loops, and vortex lines parallel to the plane. The loop behaves similar to a free ring, i.e., the radius decreases with increasing velocity, and merges into the plane at a critical velocity, $v = 1$. To comment on the flow of superfluids in real systems, we consider the effect of a surface bump. In this case, the vortex loop can either encircle or pin to the bump (again the pinned loop has a lower energy), and the vortex line acquires undulations, whose wavelength decreases with increasing flow velocity (Fig. 6). The key effect of the bump is to reduce the critical velocity, v_c (Fig. 6 lower right). In the

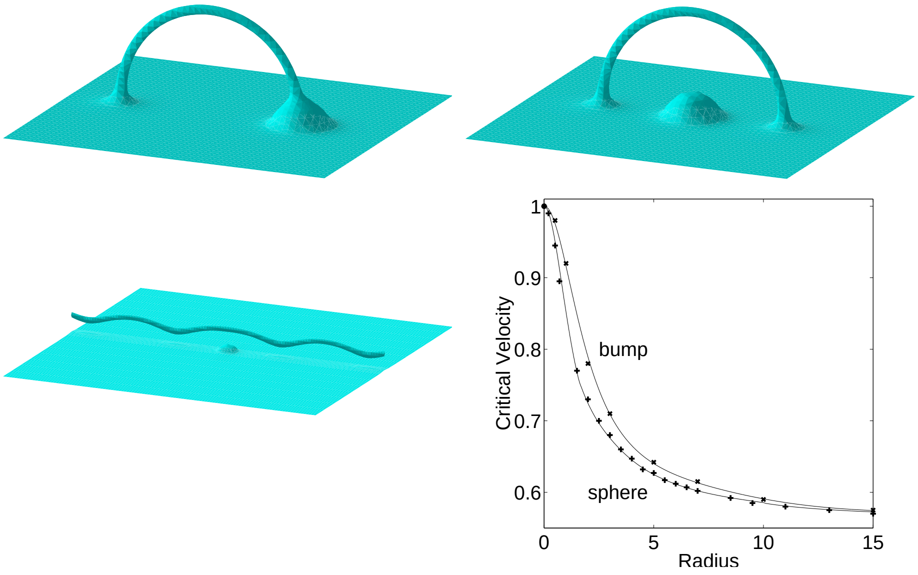

Fig. 6. – Surface density plots illustrating the stationary vortex structures near a bump on a plane surface: vortex loops pinned or encircling the bump (upper left and right) and a vortex line above the bump (lower left). The critical velocity as a function of the defect radius, R, for a hemishphere on a plane and a sphere in the bulk are shown lower right. For large R, $v_c \to 0.55$.

limit of large radius, $v_c \to 0.55$ for both surface and volume defects. As v_c coincides with the appearance of drag in superfluids, one may conjecture that surface roughness is a significant factor in determining the dissipation at low flow velocities.

Conclusions. – We have investigated vortex line and ring structures in dilute quantum fluids. We find that vortex tubes with multiple circulation consist of separate minima, and that near an object or surface lower energy, pinned solutions exist. Both laminar flow and vortex solutions become unstable at a critical velocity which is equal to the speed of sound for an unbounded flow or adjacent to a wall, but decreases near an object or surface bump. As the critical velocity corresponds to a transition between normal and drag-free flow, this dependence indicates how surface roughness can produce a marked effect on the flow of superfluids.

***

Financial support for this project was provided by the EPSRC. TW is supported by the Studienstiftung des Deutschen Volkes.

REFERENCES

[1] R. J. Donnelly, *Quantized vortices in Helium II*, (CUP, Cambridge, 1991).

[2] D. R. Tilley and J. Tilley, *Superfluidity and superconductivity*, 3rd Ed., (IoP, Bristol, 1990).

[3] M. B. Hindmarsh and T. W. B. Kibble, Rep. Prog. Phys. **58**, 477 (1995).

[4] V. L. Ginzburg and L. P. Pitaevskii, Sov. Phys. JETP **7**, 858 (1958); E. P. Gross, J. Math. Phys. **4**, 195 (1963).

[5] F. Dalfovo, S. Giorgini, L. P. Pitaevskii, and S. Stringari, Rev. Mod. Phys. **71**, 463 (1999).

[6] V. Hakim, Phys. Rev. E, **55**, 2835 (1997).

[7] C. Huepe and M.-É. Brachet, C. R. Acad. Sci. Paris, **325**, 195 (1997).

[8] T. Winiecki, J. F. McCann, and C. S. Adams, Phys. Rev. Lett. **82**, 5186 (1999).

[9] W. H. Press, S. A. Teukolsky, W. T. Vetterling and B. P. Flannary, *Numerical recipes in FORTRAN : the art of scientific computing* 2nd Ed. CUP, Cambridge, 1992.

[10] I. Aranson, and V. Steinberg, Phys. Rev. B **53**, 75 (1996).

[11] P. H. Roberts and J. Grant, J. Phys. A **4**, 55 (1971).

[12] C. A. Jones and P. H. Roberts, J. Phys. A **15**, 2599 (1982).

[13] B. Jackson, J. F. McCann, and C. S. Adams, Phys. Rev. Lett. **80**, 3903 (1998).